ORIGINAL PAPER

Detecting areas affected by flood using multi-temporal ALOS PALSAR remotely sensed data in Karawang, West Java, Indonesia

Fajar Yulianto · Parwati Sofan · Any Zubaidah · Kusumaning Ayu Dyah Sukowati · Junita Monika Pasaribu · Muhammad Rokhis Khomarudin

Abstract The normalized change index and split-based approach methods have been applied in this research to create the semiautomatic unsupervised change-detection areas affected by flood using multi-temporal Advanced Land Observing Satellite Phased Array L-band Synthetic Aperture Radar (ALOS PALSAR) remotely sensed data. This research is focused to provide information related to the flood inundation event that occurred in March 2010, in Karawang, West Java, Indonesia. The objectives of this research are as follows: (1) to generate a flood inundation map as rapid mapping steps in disaster mitigation effort and (2) to identify and assess the environmental damage caused by flood inundation event in the research area. ALOS PALSAR remotely sensed data with the acquisition pre-flood (March 09, 2010) and post-flood (March 26, 2010) were used for mapping flood inundation event. Flood inundation map and land-use data are used for the identification and assessment of the environmental damage caused by flood inundation event, which is done with GIS environment tools. The flood inundation event is estimated to have an impact of 7,158 ha for settlements; 20,039 ha for paddy fields; 668 ha for plantations; 1,641 ha for farms; 198 ha for agricultural cultivations; 1,161 ha for shrubberies; 1,022 ha for industrials; and 1,019 ha for road areas. The total number of building damages is estimated to be around 16,350 units. In general, this method can be used to assist emergency response efforts, through an inventory of areas affected by floods. In addition, the use of this method can be applied and it is recommended for future research in different locations, which are consistent and reliable to detect areas affected by other disasters such as flash floods, landslide, tsunami, volcano eruptions, and forest fire.

Keywords Remote sensing · ALOS PALSAR · Change detection · Flood inundations · Karawang · Indonesia

F. Yulianto (✉) · P. Sofan · A. Zubaidah · K. A. D. Sukowati · J. M. Pasaribu · M. R. Khomarudin
Remote Sensing Application Center, Indonesian National Institute of Aeronautics and Space (LAPAN), Jl. Kalisari No. 8, Pekayon, Pasar Rebo, Jakarta 13710, Indonesia
e-mail: fajar.lapan.rs@gmail.com; fajar.yulianto@lapan.go.id

1 Introduction

Natural disasters are natural events that can lead to adverse impact on the human population and environmental degradation. These conditions can occur in every country, and some of the impacts are usually greater experienced by the developing countries. Indonesia is one of the developing countries, which is prone to natural disasters. It lies among the Pacific tectonic plates, the Eurasian and Indo-Australian, based on the scope of geography and geology (Yulianto et al. 2013). Based on these conditions, the various types of natural disasters can occur in Indonesia, such as volcanic eruptions, earthquakes, and tsunamis. Meanwhile, some of the effects of physical and human processes can also lead to other hazards such as floods, droughts, tidal floods, land subsidence, landslides, and others (Sutikno 2007).

The Indonesian National Agency for Disaster Management, BNPB (2012), has recorded disaster events and the number of victims from 1815 to 2012 in Indonesia. The result of these records has shown that disaster events with a frequency of the highest order is flood, forest fires, cyclones, landslides, and droughts. Flood is a disaster with the highest frequency of occurrence, as many as 32 % of the total disasters in Indonesia.

Flood is defined as a current or a very high level of rivers, lakes, ponds, reservoirs, and any other water bodies, where water inundates outside of the water body area. In general, there are several factors causing flood, such as climatological events, changes in land use, increasing population, and land subsidence. Floods are the most destructive phenomena affecting the social and economic population (Smith and Ward 1998).

Karawang is one of the industrial regions in West Java, Indonesia. This area is an economic center and has industrial activities in the surrounding areas such as Jakarta, Bogor, Depok, Tangerang, Bekasi, and Bandung. A flood inundation event that occurred in March 2010 has caused more than 30,000 people to evacuate. This event has inundated ten districts and more than 16,000 houses due to the overflow from the Citarum and Cibeet River (The Regional Agency for Disaster Management (BPBD)—Province of West Java 2011).

In the implementation of disaster management practices, quick response is needed to determine the impact of disaster. The rapid mapping is necessary for emergency response in disaster mitigation effort. The methods of flood mapping based on ground surveys and aerial observation are impossible and difficult due to weather conditions. An alternative option is offered by satellite remote sensing technology (Brivio et al. 2002).

Optical remote sensing data with passive sensor have been used in several researches for mapping the flood inundation. These researches were conducted with several approaches, involving digital or visual analyses such as those carried out by Brivio et al. (1984) using Landsat Multispectral Scanner (MSS); Lougeay et al. (1994), Pantaleoni et al. (2007), Yueming et al. (2007) using Landsat Thematic Mapper (TM); Blasco et al. (1992) using SPOT XS; Quan et al. (2003); Billa et al. (2006), Sanjay et al. (2006), Kuligowski (2011) using NOAA AVHRR; and Brakenridge and Anderson (2006), Shifeng et al. (2012) using MODIS remote sensing data. However, optical remote sensing data cannot show the surface condition when it is covered by clouds. Adverse weather conditions during and after flood events are constraints to the utilization of optical remotely sensed data. Cloud cover and atmospheric conditions are major constraint in the use of these data, so they can be prohibitive in identifying land surface objects (Dong et al. 2010; Yulianto et al. 2013). Synthetic aperture radar (SAR) remote sensing data with active sensors can be used to solve the problems contained in an optical remote sensing data. These data can penetrate clouds and give the surface information clearly. Several researches have been conducted in

identifying flood using SAR remote sensing data, such as Townsend (2001), Bovolo and Bruzzone (2007), Huang et al. (2011) using RADARSAT; Bazi et al. (2005) using European remote sensing (ERS); Moser and Serpico (2006) using SAR X-band and space borne radar image C-band; and Martinis et al. (2009), Mason et al. (2010) using TerraSAR-X. The results of these studies indicate that the SAR remote sensing data could be used effectively for identifying and detecting areas affected by floods. In addition, the uses of SAR remote sensing data could be used as an alternative to replace the availability and problems continued on optical remote sensing data.

Change detection is the process of identifying differences in the state of an object or phenomenon by observing it at different times. Essentially, it involves the ability to quantify temporal effects using multi-temporal data set (Singh 1989). This method could also be applied to detect and assess natural disasters such as earthquake, floods, mud-rock flows, and forest fires. Several other applications have been applied by Tzeng et al. (2009); Wulder et al. (2008); and Bayarsaikhan et al. (2009). SAR is strongly sensitive to the surface change caused by disaster damage. The damage detection from SAR remote sensing data requires pre- and post-disaster acquisition (Dong et al. 2010). In this research, change detection could also be applied to create flood inundation map and assess the environmental damage due to flood event in research area.

A split-based approach (SBA) for the semiautomatic unsupervised change-detection area in multi-temporal SAR remote sensing data is applied, which originally has been proposed by Bovolo and Bruzzone (2007). In such research, SBA is used for unsupervised change-detection area in large-size multi-temporal RADARSAT-1 remotely sensed data and it is applied to tsunami damage assessment. The use of SBA was designed and developed to identify the tsunami damage in coastal areas of Sumatera Island, Indonesia. The change detecting area is done by taking into account the difference or ratio image on multi-temporal RADARSAT-1 (pre- and post-tsunami). The results of these calculations are used as a basis for the SBA, which is used to determine the threshold value in making the change-detection map. The results from these studies indicate that the use of multi-temporal RADARSAT-1 increases the effectiveness of the proposed SBA and can be used as a system for tsunami damage assessment applications. The use of the same method has also been performed by Martinis et al. (2009) for the identification of flood in the River Severn, UK; a change-detection area by flood is applied using high-resolution TerraSAR-X remotely sensed data. Backscattering change in SAR remote sensing data can be calculated using the normalized change index (NCI), which is used as the basis for determining the SBA. The results showed that the classification of the areas "flood" and "non-flood" from the use of TerraSAR-X of the proposed SBA in combination with optical image segmentation and integration of digital elevation models has high-accuracy values.

In this research, the use of NCI and SBA methods such as that has been done by Martinis et al. (2009). It was applied for detecting areas affected by flood in the medium-size-resolution multi-temporal Advanced Land Observing Satellite Phased Array L-band Synthetic Aperture Radar (ALOS PALSAR) remotely sensed data in Karawang, West Java, Indonesia. The determination of the threshold value based on the Kittler and Illingworth (KI) approach with minimum error principle is used in object classes "flood" and "non-flood" from the calculation of NCI and SBA. This research focuses on providing information-related flood inundation event in Karawang on March 2010. The objectives of this research are as follows: (1) to generate a flood inundation map as rapid mapping steps in disaster mitigation effort, (2) to identify and assess the environmental damage caused by flood inundation event in the research area.

2 Study area

Karawang is positioned at the coordinates of about at 5°56′ to 6°34′S and 107°02′ to 107°40′E (Fig. 1). It is one of the industrial regions in Indonesia and situated in West Java. This area is an economic center and has industrial activities in the surrounding areas such as Jakarta, Bogor, Depok, Tangerang, Bekasi, and Bandung. The city consists of 30 districts and covers an area of approximately 1,753.27 km^2, with a population of 2,127,791 people in 2010. Table 1 shows the information, data about regional area, number of population, and population density and distribution in Karawang (Statistic of Karawang 2011).

Regionally, Karawang can be divided into two major landscapes, namely lowland and coastal area on the northern part with elevations ranging from 0 to 50 m and a hilly area on the southern part with elevation from 50 to 1,291 m above mean sea level. The city center is situated in the lowland area, and it is growing rapidly in line with the increasing population. The meteorological condition of the Karawang area consists of a temperature range between 25.8 and 27.0 °C with an annual humidity of 66–80 % and a mean-annual wind velocity of 30–35 km/h. The annual rainfall is about 1,677–2,534 mm, and the maximum rainfall occurs in the months of December and January. The dominant geological materials in Karawang are sedimentary rock and alluvial sediment. Sedimentary rock from marine origin consists of clay and stone that is dominated by sandstone. Alluvial sediment consists of beach and fluvial deposits formed from clay and sand. Karawang has
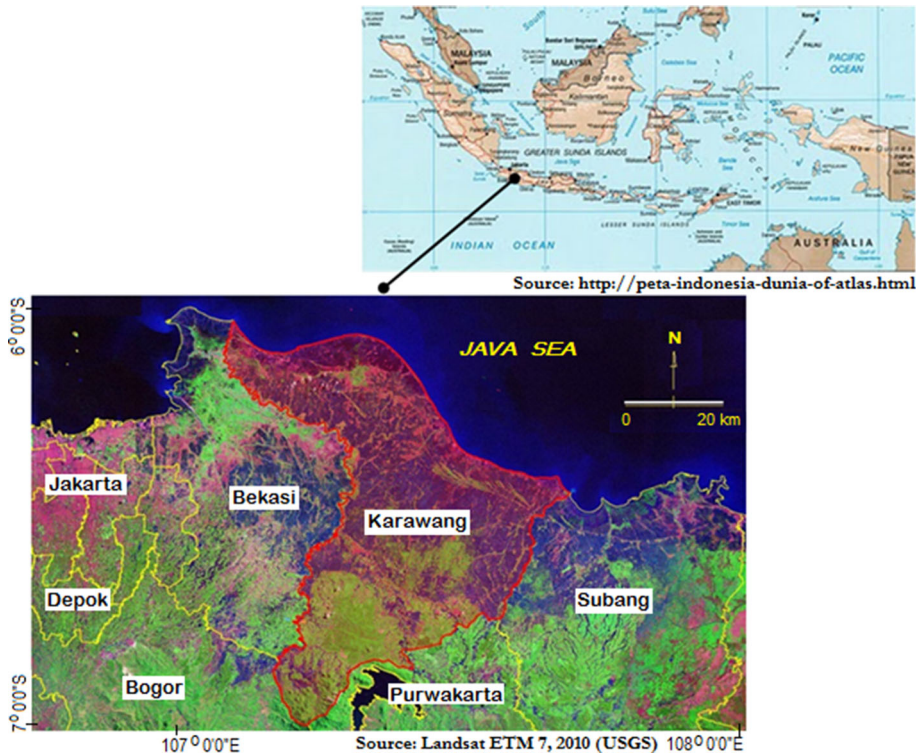

Fig. 1 Research area at Karawang, West Java, Indonesia

Table 1 Regional area, number of population, population density, and distribution in Karawang

No.	Districts	Area (km²)	Number of population	Density per km²	Distribution (%)
1	Pangkalan	94.37	35,245	373.48	1.66
2	Tegalwaru	86.34	34,154	395.58	1.61
3	Ciampel	110.13	39,340	357.21	1.85
4	Telukjambe Timur	40.13	126,616	3,155.15	5.95
5	Telukjambe Barat	73.36	48,803	665.25	2.29
6	Klari	59.37	155,336	2,616.41	7.30
7	Cikampek	47.60	107,020	2,248.32	5.03
8	Purwasari	29.44	63,274	2,149.25	2.97
9	Tirtamulya	35.06	44,274	1,262.81	2.08
10	Jatisari	53.28	72,003	1,351.41	3.38
11	Banyusari	55.30	51,012	922.46	2.40
12	Kotabaru	30.45	119,710	3,931.36	5.63
13	Cilamaya Wetan	69.36	75,318	1,085.90	3.54
14	Cilamaya Kulon	63.18	59,780	946.19	2.81
15	Lemahabang	46.91	60,758	1,295.20	2.86
16	Telagasari	45.72	60,163	1,315.90	2.83
17	Majalaya	30.09	44,016	1,462.81	2.07
18	Karawang Timur	29.77	118,001	3,963.76	5.55
19	Karawang Barat	33.68	155,471	4,616.12	7.31
20	Rawamerta	49.43	48,657	984.36	2.29
21	Tempuran	88.09	58,608	665.32	2.75
22	Kutawaluya	48.67	53,741	1,104.19	2.53
23	Rengasdengklok	31.46	104,494	3,321.49	4.91
24	Jayakerta	41.24	59,929	1,453.18	2.82
25	Pedes	60.84	70,168	1,153.32	3.30
26	Cilebar	64.20	39,421	614.03	1.85
27	Cibuaya	87.18	48,660	558.16	2.29
28	Tirtajaya	92.25	61,919	671.21	2.91
29	Batujaya	91.89	75,336	819.85	3.54
30	Pakisjaya	64.48	36,564	567.06	1.72
Total		1,753	2,127,791	1,214	100

Source: DPB (2011) and Statistic of Karawang (2011)

two major rivers flowing to the north. The rivers are Cibeet and Citarum River. Cibeet River is located in the western part and flows from south to Citarum River, and it is an administrative boundary between Karawang and Bekasi. Meanwhile, Citarum River is located in the eastern part flowing north, and it is an administrative boundary between Karawang and Subang (Development Planning Board, DPB 2011).

Rainfall conditions in the research area during flood event March 23, 2010 can be shown based on the rainfall accumulation from QMorph remotely sensed data on March 22–25, 2010. Figure 2 shows the accumulation of rainfall from QMorph remotely sensed data in the research area (Citarum Watershed) on March 22–25, 2010, time: 00–23
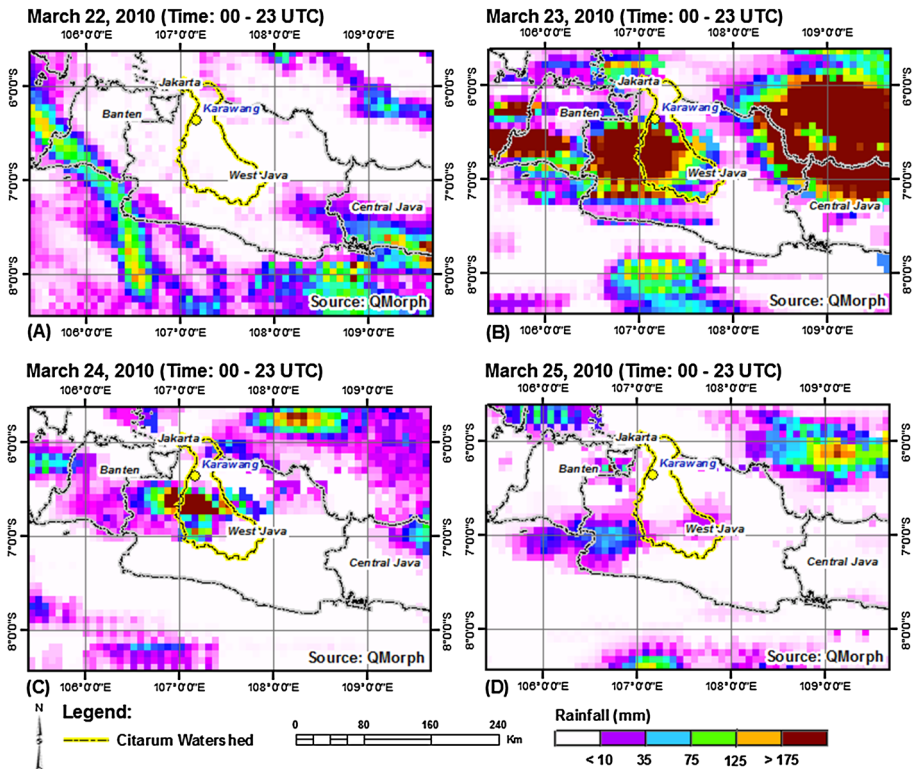
Fig. 2 Rainfall accumulation based on QMorph remotely sensed data in the research area (Citarum Watershed), on March 22–25, 2010. **a** Rainfall accumulation on March 22, 2010, time: 00–23 UTC. **b** Rainfall accumulation on March 23, 2010, time: 00–23 UTC. **c** Rainfall accumulation on March 24, 2010, time: 00–23 UTC. **d** Rainfall accumulation on March 25, 2010, time: 00–23 UTC (*source*: QMorph remotely sensed data, processed by: LAPAN 2010)

Coordinated Universal Time (UTC). The monitoring results show that on March 23–24, 2010, the accumulation of rainfall in the research area is more than 175 mm for time: 00–23 UTC. The existence of these conditions for 2 days with a relatively long duration of time has triggered flood in the research area.

3 Data

3.1 Generate a flood inundation map

ALOS PALSAR remotely sensed data on the acquisition of pre-flood (March 09, 2010) and post-flood (March 26, 2010) with 30 m spatial resolution were used for mapping of the flood inundation in research area (Table 2). Furthermore, the result of flood inundation map was used for the identification and assessment of the environmental damage areas caused by flood with the GIS environment tools.

Table 2 Information of ALOS PALSAR remotely sensed data with HH polarization and descending track direction used in this research

Scene ID	Date time	Incidence angle
ID_ALPSRP_219617050	March 09, 2010 15:42:36	34.3
ID_ALPSRP_219617060	March 09, 2010 15:42:44	34.3
ID_ALPSRP_222097050	March 26, 2010 15:44:37	36.9
ID_ALPSRP_222097060	March 26, 2010 15:44:45	36.9

3.2 Identification and assessment of the environmental damage due to flood inundation event

Land-use data in the year 2010 with scale of 1:25,000 was obtained from the Indonesian National Institute of Aeronautics and Space (LAPAN) which is used to describe the condition of land-use information in the research area. Topographic map in the year 1998 with scale 1:25.000 was obtained by the Geospatial Information Agency (BIG) which is used as a base map and used to describe the number of building sites in the research area. Geo Eye satellite data from Digital Globe Google map in the year 2010 are used to update the points of the building site topographic map in 1998.

4 Methodology

In general, the flowchart of methodology for this research can be seen in Fig. 3. The data processing and analysis were divided in two steps: (1) generating flood inundation map as rapid mapping steps in disaster mitigation effort, (2) identification and assessment of the environmental damage due to flood inundation events in the research area. Detailed description of the methodology steps undertaken in this research is given in the following sections.

4.1 Preprocessing and radiometric calibration

Preprocessing stage in this research consists of geocoding and radiometric calibration. At this stage, geocoding is required for converting the images, which have geocoded information from the global Cartesian coordinates system (geographic coordinate system) into
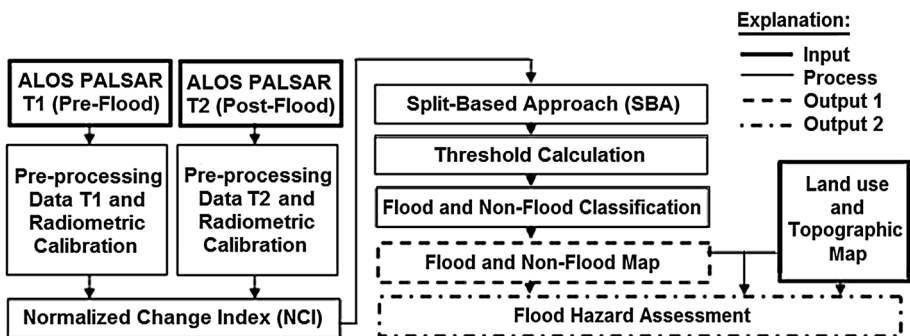

Fig. 3 Flowchart of the research

the local cartographic reference system (Universal Transverse Mercator). ALOS PALSAR remotely sensed data are used to provide information about the gray-level intensity in a digital number (DN). A radiometric calibration process was carried out with the aim of converting the digital number value in the image into the backscattering coefficient called sigma nought (σ^0). Sigma nought serves to determine the value of the backscattering in the reflection of an object in dB. Formula to calculate the value of the coefficient sigma nought is presented in Eqs. (1) and (2). It was used to obtain sigma nought in dB (Dong et al. 2010; Yulianto et al. 2013).

$$\sigma_{i,j}^0 = K \cdot \mathrm{DN}_{i,j}^2 \, (i = 1, 2, \ldots, L; \quad j = 1, 2, \ldots, M) \tag{1}$$

$$\sigma_{i,j}^0(\mathrm{dB}) = 10 \log_{10}\left(\sigma_{i,j}^0\right) = 20 \log_{10}(\mathrm{DN}) + K(\mathrm{dB}) \tag{2}$$

where K is an absolute calibration constant, $\mathrm{DN}_{i,j}^2$ is a pixel intensity value at image line i and column j, $\sigma_{i,j}^0(\mathrm{dB})$ is a backscattering coefficient sigma nought at image line i and column j in dB, and L and M are numbered of line and column in the product. The value of calibration constant for data processed ALOS PALSAR remotely sensed data is -83, which is provided by Japan Aerospace Exploration Agency (JAXA).

4.2 Normalized change index (NCI)

In this research, change detection can be calculated with normalized change index (NCI). Calculation of NCI is used as an indicator of changes in the land surface caused by flood inundation event. ALOS PALSAR remotely sensed data acquisition $T1$ (pre-flood) and $T2$ (post-flood) were required for determining land surface change in the calculation of NCI. Formula for determining the NCI can be seen in Eq. (3) (Martinis et al. 2009):

$$\mathrm{NCI} = \left(\left(\sigma_{\mathrm{post}} - \sigma_{\mathrm{pre}}\right) / \left(\sigma_{\mathrm{post}} + \sigma_{\mathrm{pre}}\right)\right) + 1 \tag{3}$$

where NCI is the calculation of normalized change index on data acquisition $T1$ and $T2$. σ_{pre} is the value of backscattering data acquisition $T1$ (pre-flood). σ_{post} is the value of backscattering data acquisition $T2$ (post-flood).

NCI has a float data range from [0, …, 2], with values that are equal to one showing the unchanged areas. A high NCI is an indicator for pixels with an increase in backscattering at $T2$, which, in this case, is related to changes caused by decreasing the flood level. For a more efficient data handling, the float values of NCI are transformed to 8-bit integers with a possible gray-level range [0, …, 256].

4.3 Split-based approach (SBA)

Split-based approach (SBA) for unsupervised flood detection in SAR data is applied, which originally has been proposed by Bovolo and Bruzzone (2007) for the identification of tsunami-induced changes in multi-temporal imagery. This method has been used by Martinis et al. (2009) for flood identification using TerraSAR-X remotely sensed data. Flood and non-flood classes can show different probabilities when applied to the entire scene data. SBA is used to determine the local threshold variations due to the limited capability of the global threshold for the classification of flood and non-flood in the entire scene data. The SBA can be described with illustrations of scene images that have a dimension in size $P \times Q$. Figure 4a shows the grid cells with the size of the scene image
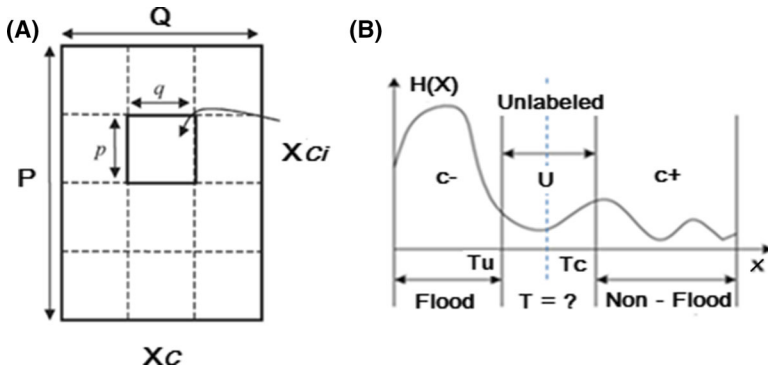
Fig. 4 a Grid cells with the size of the scene image $P \times Q$ and sub-scene images X_{Ci} with size $p \times q$ (*source*: Bovolo and Bruzzone 2007). **b** The graphic illustration of the distribution of pixel values in a class of flood ($C-$) and non-flood ($C+$) (*source*: Huang et al. 2011)

$P \times Q$ and sub-scene images X_{Ci} with size $p \times q$. $P \times Q$ is a grid cell in one scene image. P is a line in one scene image $P \times Q$. Q is a column in one scene image $P \times Q$. X_{Ci} is sub-scene image X_C to i where ($i = 1, 2, 3, \ldots, n$). p is one of the split parts of the line sub-scene image X_{Ci}. q is one of the split parts of the column sub-scene image X_{Ci} (Bovolo and Bruzzone 2007).

In this research, the result of NCI image is used to implement split scene image with size $P \times Q$. Distribution split scene image into several sub-scene images are not limited in the number of distributions. In general, the threshold algorithm only can be used to extract proper threshold values if the histogram is not unimodal. Thus, the selection process must be emphasized that the sub-scene image must consist of pixels that belong to a class of flood and non-flood. At least 10 % of each of the two classes are in a sub-scene image (Bazi et al. 2005; Bovolo and Bruzzone 2007; Martinis et al. 2009). Determination of SBA or scene selection sub-scene image carried out by statistics. Detailed technical information on the use of the SBA method can be explained on the research that has been done by Martinis et al. (2009).

4.4 Threshold calculation to flood and non-flood classification maps

The determination of the threshold value is used in object classes, flood and non-flood, from the calculation of NCI and SBA. In this research, the object classes are divided into two classes (Fig. 4b), namely flood ($C-$) and non-flood ($C+$). Figure 4b shows the graphic illustration of the distribution of pixel values in a class of flood ($C-$) and non-flood ($C+$). The results of the flood and non-flood classes are not directly fallen into two classes required, as there are classes unlabeled or (U). Unlabeled class is a class where there is a refractive range of pixel values ($C-/U$) and ($C+/U$). T_U is a boundary between ($C-$) and (U) or can be referred to as ($C-/U$). T_C is a boundary between ($C+$) and (U) or can be referred to as ($C+/U$) (Huang et al. 2011). In this research, the histogram of the ALOS PALSAR remotely sensed data can be assumed to be a statistical model by the two 1-D normal distributions of flood and non-flood class [$p(g|i)$, $i = \{1:$ flood, $2:$ non-flood$\}$]. This model has parameters such as: probability (P_i), mean (μ_i), and standard deviation (σ_i). The boundary between classes flood and non-flood in an unlabeled class is determined by the threshold value (T). The calculation of the threshold value is based on the Kittler and

Illingworth (KI) approach with minimum error principle. Detailed technical information on the use of method of KI approach with minimum error principle can be explained on the research that has been done by Kittler and Illingworth (1986); Bazi et al. (2005); Martinis et al. (2009).

4.5 Identification and assessment of the environmental damage due to flood inundation event

The limitation from the use of the word "environmental damage" in this research is focused on the calculation of the amount of land-use area affected by flood, which is expected to provide information on the environmental conditions of the study area. This research has applied the methods of cross-profile and rapid field observation to identify the impact of flood inundation event on the environment. Cross-profile in this research was used to describe the cross section of the vertical and horizontal position of a region. The condition of the region can be described well, by looking at the vertical and horizontal position of an area. Comprehensive conditions of the region may include variations in topographic information, land use, landform units, and other environmental physical parameters. Some data, photographs, and other supporting surveys, such as local community information, newspapers, and relevant agencies, are required in this research to provide an overview of the current conditions of the research area affected by floods. This method is best used to describe and represent the environmental impact of disaster in the region (Marfai 2011; Yulianto et al. 2013).

The assessment of the impact of disasters can be done by overlaying the map of disaster with the land-use map to determine the number of damages events, as has been done by Marfai and King (2008); Ward et al. (2011); Marfai (2011); Yulianto et al. (2013). In this research, assessment of the flood hazard on the environmental requires land-use and information points of the building site. In order to calculate the flood hazard assessment, an overlay method in a GIS environment was done by integrating the flood inundation event, land-use map, and information points of the building site topographic map. The process can be done by converting raster to vector data in flood inundation map, which describes a class of flood and non-flood. Furthermore, the conversion result can be overlaid with the land use and points of the building site topographic map for the identification and assessment of the environmental damage due to flood inundation event in the research area.

5 Results and discussion

5.1 The characteristic of backscattering value and generating a map of flood inundation event in the research area

Flood inundation has occurred in Karawang on March 23, 2010. Rapid mapping is required to determine the distribution of inundation and flood hazard assessment in the research area. ALOS PALSAR remotely sensed data pre-flood (March 09, 2010) and post-flood (March 26, 2010) were used in this research for mapping of flood inundation event. Figure 5 shows that ALOS PALSAR remotely sensed data pre- and post-flood are used in this research.

It can be seen from Fig. 5a, b that the backscattering coefficient sigma nought (σ^0) on the pre-flood data has a range of value 0.001–7.29 dB. Meanwhile, the backscattering coefficient sigma nought (σ^0) on the post-flood data has a range of value 0.001–17.33 dB.
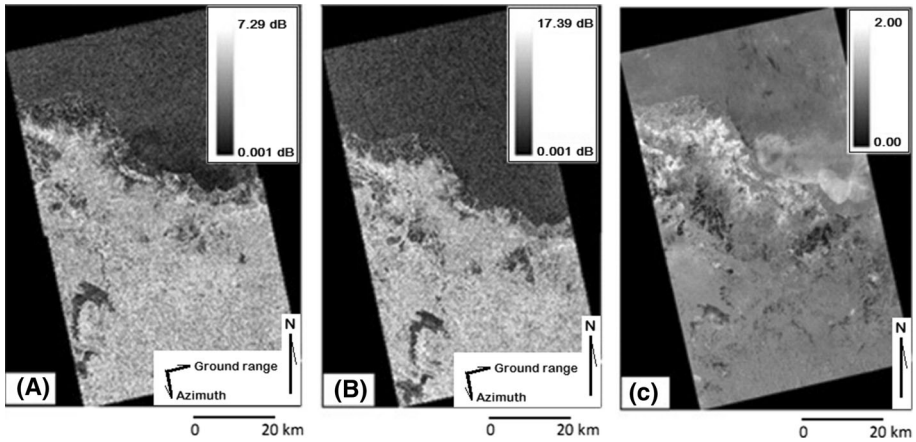
Fig. 5 ALOS PALSAR remotely sensed data pre- and post-flood used in this research. **a**, **b** The result of radiometric calibration DN value into backscattering coefficient sigma nought (σ^0) on the mosaic of pre- and post-flood data. **a** ALOS PALSAR remote sensing data March 09, 2010 (pre-flood) mosaic of scene data: ID_ALPSRP_219617050 and ID_ALPSRP_219617060. **b** ALOS PALSAR remote sensing data March 26, 2010 (post-flood) mosaic of scene data: ID_ALPSRP_222097050 and ID_ALPSRP_222097060. **c** Result of normalized change index (NCI) in dB based on the calculation of data pre- and post-flood inundation event

This value indicates that the lower value of backscattering coefficient sigma nought is due to the condition of land surface that is dark. It is caused by the weak backscattering signal that was returned to the SAR sensor. Meanwhile, the higher value of backscattering co-efficient sigma nought is due to the land surface condition that is brighter, related to the strong backscattering signal that returns to the SAR sensor.

In the research area, the characteristic of backscattering value can be distinguished based on the types of land-use areas affected by floods (Fig. 6; Table 3). Figure 6 shows the characteristics of backscattering of ALOS PALSAR remotely sensed data ($T1$ pre-flood) and ($T2$ post-flood) on the types of land-use areas affected by floods in the research area. The vertical axis shows backscattering value in dB, and the horizontal axis shows types of land-use areas affected by floods in the research area. From Fig. 6, it can be seen that each of the types of land use has value different backscattering at the before and after floods. At the before floods, the objects of the land use are likely to have higher backscattering value than at the after floods. This occurs because of the characteristic of object roughness and the backscattering on land use is near acceptable SAR sensor and not been affected by the flood inundations. Table 3 shows the result of the calculations and the characteristic of backscattering ALOS PALSAR remotely sensed data ($T1$ pre-flood and $T2$ post-flood) on the types of land-use areas affected by floods. It can be seen from Table 3 that land-use types of industrial and settlement have higher different backscattering values at the before and after floods: 0.70 and 0.62. While the land-use types of plantations, paddy fields, agricultural cultivations, and shrubberies have lower different backscattering values: 0.17, 0.16, 0.14, and 0.12, respectively.

Some locations are experiencing changes of the backscattering value, which can be rapidly and effectively done using a calculation of NCI. Changes of the backscattering value are due to the flood inundation in the research area. The uses of NCI calculation can be relatively quick and efficient due to the backscattering ability to describe changes in the location of the affected flood inundation. Figures 5c and 7a show the results of the change-
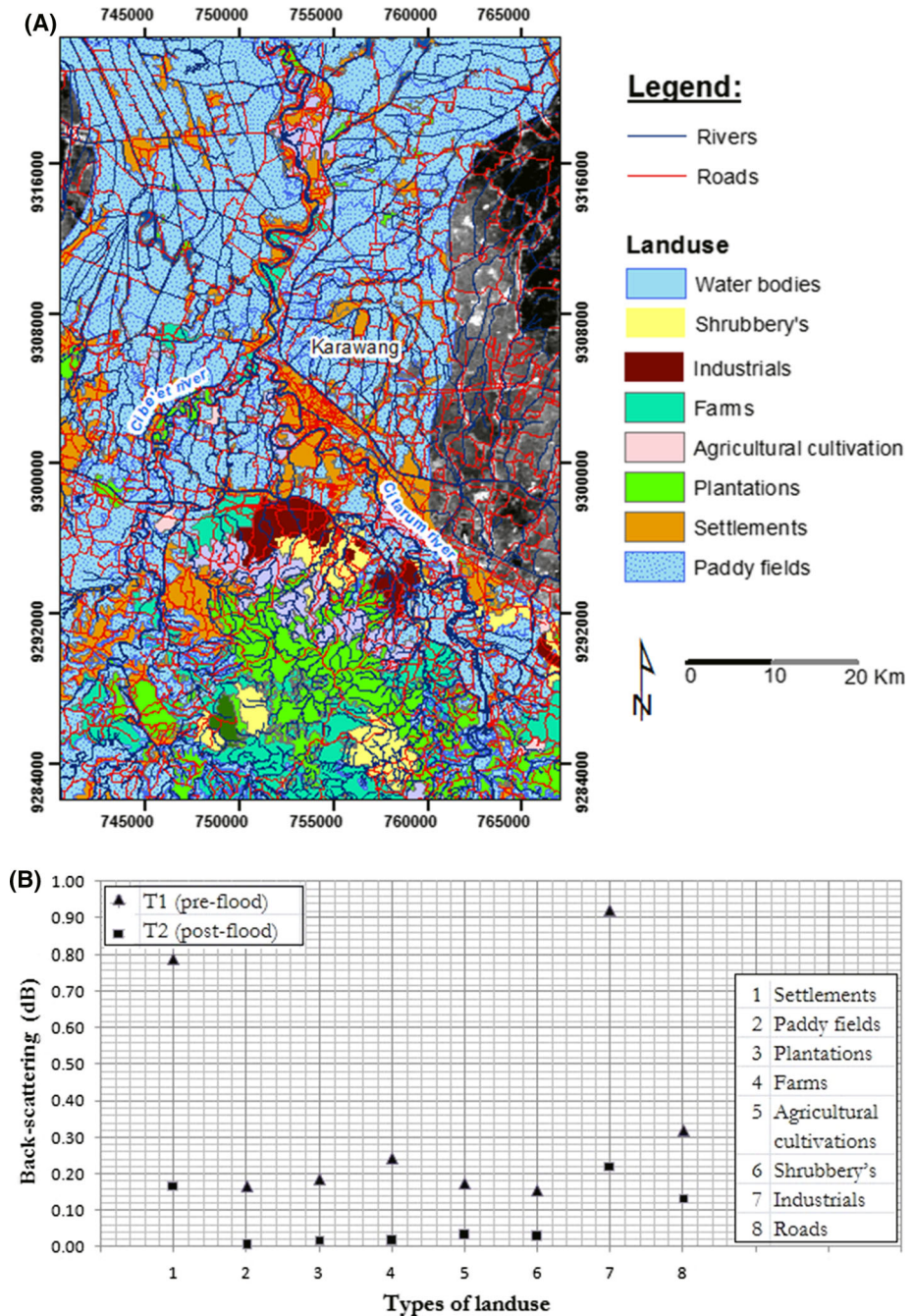
Fig. 6 **a** Types of land use in the research area. **b** Characteristics of backscattering ALOS PALSAR remote sensing data (*T1* pre-flood) and (*T2* post-flood) on the types of land-use areas affected by floods in the research area

Table 3 Calculations and characteristic of backscattering ALOS PALSAR remotely sensed data acquisitions ($T1$ pre-flood) and ($T2$ post-flood) on the types of land-use areas affected areas by flood in the research area

No.	Types of land use	$T1$ (pre-flood)	$T2$ (post-flood)	$\Delta T = T1 - T2$
1	Settlements	0.79	0.17	0.62
2	Paddy fields	0.17	0.01	0.16
3	Plantations	0.19	0.02	0.17
4	Farms	0.24	0.02	0.22
5	Agricultural cultivations	0.17	0.03	0.14
6	Shrubberies	0.15	0.03	0.12
7	Industrials	0.92	0.22	0.70
8	Roads	0.32	0.13	0.19

detection approach using the calculation of NCI method. From Fig. 5c, it can be seen that result of NCI has a range value 0.00–2.00, which shows the range value of changed areas. This value indicates that the smaller values of NCI approximate 0.00 value or dark colors; the chances of a change in surface area due to flood are greater. Meanwhile, the greater values of NCI approximate 2.00 value or bright colors; the chances of a change in the land surface area due to flood are smaller. A high NCI is an indicator for pixels with an increase in backscattering at $T2$, which, in this case, is related to changes caused by decreasing of the flood level. The float values of NCI are transformed to 8-bit integers with a possible gray-level range [0, …, 256], for a more efficient data handling (Fig. 7a).

Determination of split-based approach (SBA) is done in one scene image of NCI with a value of gray-level range [0, …, 256]. Figure 7b shows the results of SBA determination in grid cells with the size of the scene image $P \times Q$ and sub-scene images X_{Ci} with size $p \times q$. It can be seen from Fig. 7b that a total of 5,063 grid cells (red color grid) is made with size 500×500 pixels, then chosen as 1,737 grid cells (blue color grid) that covers a land area of research (masking area for water bodies object such as sea, lakes, and reservoirs).

Selection of sub-scene image for further analysis is performed statistically. The calculation was based on the value of the coefficient of variation on each sub-scene image, which is the ratio between the mean values and standard deviation. The result of calculation plots statistical parameter SBA, which can be seen in Fig. 7c. The vertical axis shows ratio scene parameter, and the horizontal axis shows the coefficient of variation parameter from each sub-scene image. This plot statistical parameter is used to select sub-scene image of the most suitable and can be used as an indicator of the chances of the two classes in a sub-scene image. The smaller coefficient of variation and ratio scene value in a sub-scene image can be used as an indicator for the chances of increases in two different classes. The greater the coefficient of variation and ratio scene value, then the chances of the existence of two different classes are smaller. Figure 8 shows result and locations of determination of sub-scene image (X_n'). It can be seen from Fig. 8 that those criteria for determination of sub-scene image (X_n') in the research area are done by looking at the value of the coefficient of variation >0.7 and the ratio scene value between 0.4 and 0.9. Based on these criteria, as much as 15 grid sub-scene images X_1', X_2', X_3', …, X_{15}' are obtained. Figure 9 shows result and locations of determination of sub-scene image (X_n''). These grid sub-scene images (X_n') were used to determine the sub-scene image (X_n'') with
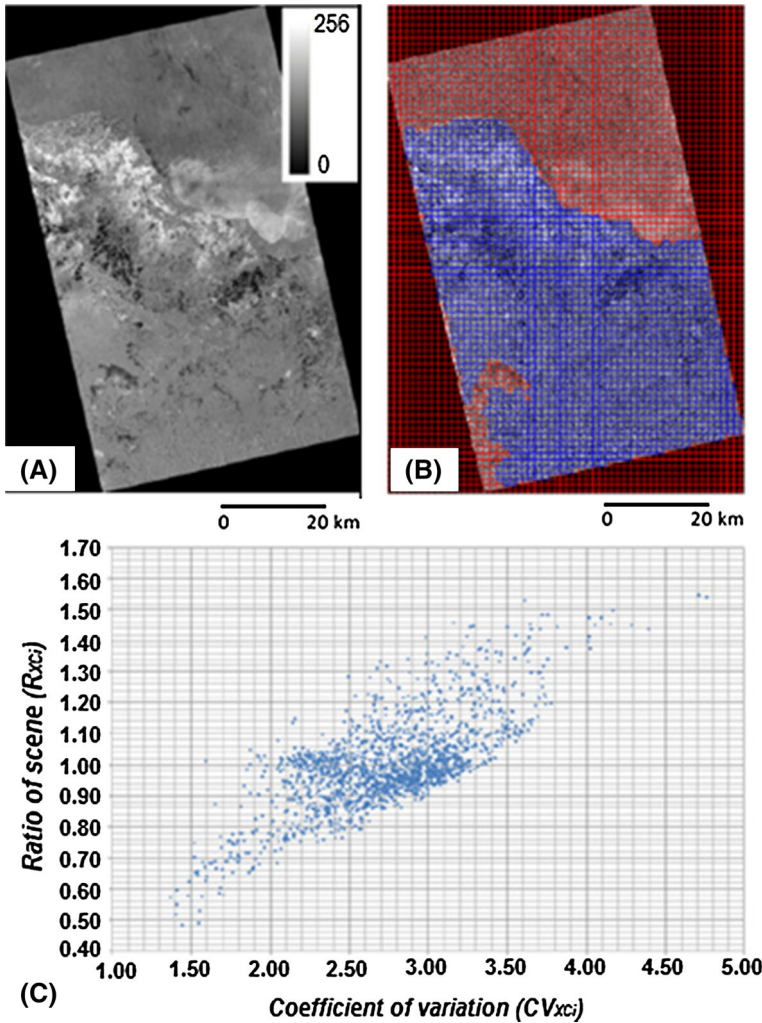
Fig. 7 **a** Result of normalized change index (NCI), **b** split-based approach (SBA), and **c** plots of the statistical parameter SBA. **a** NCI based on the calculation of data pre- and post-flood inundation event. The float values of NCI are transformed to 8-bit integers with a possible gray-level range [0, …, 256]. **b** SBA based on creating a grid of size $p \times q$ sub-scene image X_{Ci} in one scene image of NCI. A total of 5,063 grid cells (*red color grid*) is made with size 500 × 500 pixels, then chosen as 1,737 grid cells (*blue color grid*) that cover a land area of research. **c** Plots data based on value parameter SBA, coefficient of variation (in axis X), and ratio of scene (in axis Y)

calculation the Euclidean distance nearest from each the value coefficient of variation (in axis X) and ratio scene (in axis Y). Based on result calculation of the Euclidean distance, as much as 8 grid sub-scene images X_1'', X_2'', X_3'', …, X_8'' are obtained.

The results of calculation on sub-scene image X_1'', X_2'', X_3'', …, X_8'' are used to determine threshold values for object classes flood and non-flood. Table 4 and Fig. 10 show the calculation of threshold value, and the result of object classification of flood and non-flood is based on the Kittler and Illingworth (KI) approach with minimum error
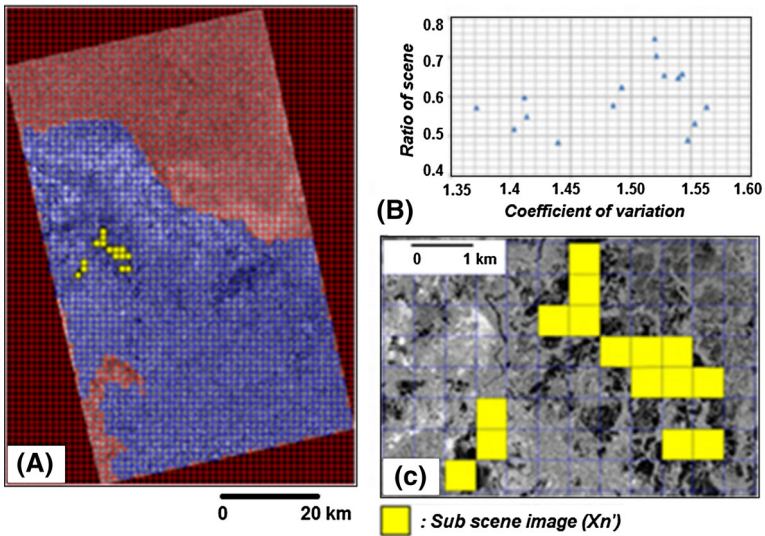
Fig. 8 Result of determination of sub-scene image (X_n'). **a** Inset location of sub-scene image (X_n') with a background of SBA based on creating a grid of size $p \times q$ sub-scene image X_{Ci} in one scene image of NCI. **b** Plots data based on value parameter SBA, coefficient of variation (in axis X) and ratio scene (in axis Y), with criteria the value of the coefficient of variation >0.7 and the ratio scene value between 0.4 and 0.9. **c** Grid location of sub-scene image (X_n')
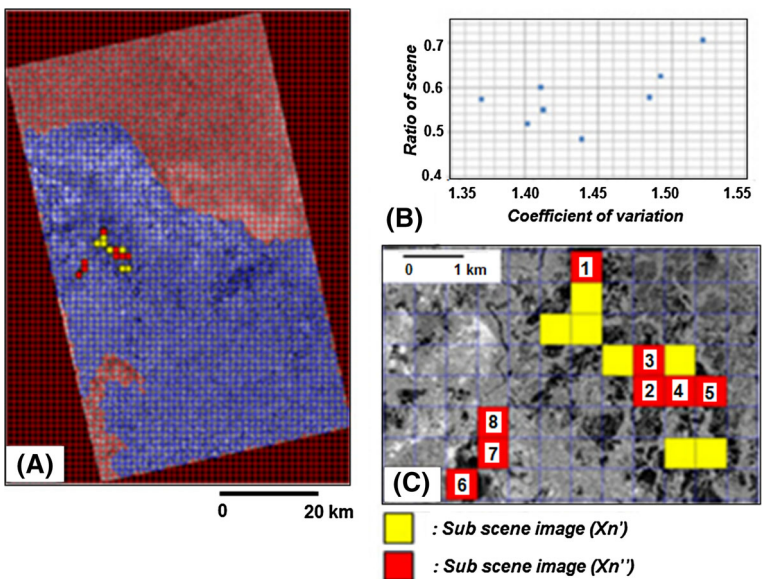
Fig. 9 Result of determination of sub-scene image (X_n''). **a** Inset location of sub-scene image (X_n') with a background of SBA based on creating a grid of size $p \times q$ sub-scene image X_{Ci} in one scene image of NCI. **b** Plots data based on calculating the Euclidean distance nearest from each the value coefficient of variation (in axis X) and ratio scene (in axis Y) in all sub-scene images. **c** Grid location of sub-scene image (X_n'')

Table 4 Calculation of the threshold value is based on the Kittler and Illingworth (KI) approach with minimum error principle for the split sub-scene image (X_n'')

No.	Sub-scene image (X_n'')	Probability		Mean		Standard deviation		Threshold (KI)
		P_1	P_2	μ_1	μ_2	σ_1	σ_2	
1	X_1''	0.49	0.51	506.28	139.35	92.63	87.02	67
2	X_2''	0.46	0.54	460.71	149.44	79.91	79.42	68
3	X_3''	0.44	0.66	456.84	152.06	84.08	84.05	67
4	X_4''	0.53	0.47	509.99	126.12	113.51	76.77	73
5	X_5''	0.52	0.48	485.96	128.80	88.39	86.96	75
6	X_6''	0.43	0.57	426.23	155.30	71.55	62.47	70
7	X_7''	0.26	0.74	242.28	201.89	28.36	69.88	72
8	X_8''	0.25	0.75	240.95	202.27	56.20	70.31	73

Where $p(g|i)$, $i = \{1: \text{flood}, 2: \text{non-flood}\}$

principle for the split sub-scene image (X_n''). It can be seen from Table 4 that the variation of the local threshold ranges from 67 to 75 in 8-bit integers. From Fig. 10, it can be seen that the object classification of flood and non-flood is done by calculating the threshold value. The blue color is a result of flood classification, and red color is a result of non-flood classification. Table 5 shows the results of local threshold for the determination of global threshold value. Mean and median values obtained as threshold combining from 8 sub-scene images were 70.6 and 71.0 with threshold merging as a global threshold value 70.6. Threshold value 70.6 is a global threshold used to create maps of flood inundation. Figure 11 shows a map of flood inundation in the research area. It can be seen from Fig. 11 that flood inundation spread on four main locations in research area, namely district of Batujaya, Rawamerta, Karawang, and Telukjambe.

5.2 Identification and assessment of the environmental damage due to flood inundation event

Identification of the environmental damage due to flood inundation event in research area has applied the methods of cross-profile and rapid field observation. Some data, photographs, and other supporting surveys, such as local community information, newspapers, and relevant agencies are required in this research to provide an overview on the current conditions of areas affected by floods. Assessment of the flood hazard on environmental requires land-use and information points of the building site. To calculate of the flood hazard assessment, an overlay method in a GIS environment mapping of flood inundation event, land-use map, and information points of the building site topographic map was applied.

Cross-profiling and difference backscattering value pre- and post-flood have been designed for six transect routes representing entire research areas (Fig. 12). Meanwhile, the backscattering interaction of water and land surface between the SAR signal is presented in Fig. 13. The interaction between the SAR signal with water and land surface by Martinis (2010) can be categorized into: specular reflection, corner reflection, diffuses surface scattering, diffuse volume scattering, and Bragg scattering. In this research, ALOS PAL-SAR remotely sensed data backscattering signal interaction between water (flood) and the land surface (land use) at each cross-profile is generally included in the category of
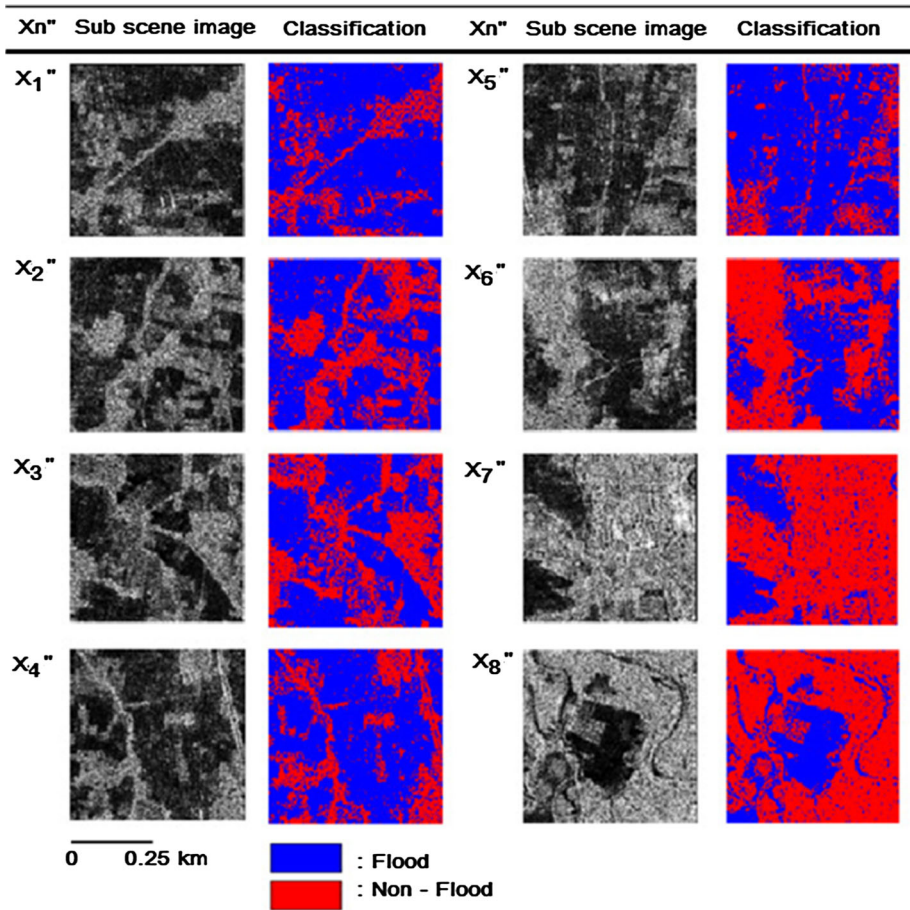
Fig. 10 Result of classification of flood and non-flood inundation in sub-scene image (X_n'') using calculation of Kittler and Illingworth (KI) approach

Table 5 Result of the local threshold calculated by Kittler and Illingworth (KI) algorithm for the determination of global threshold value

Sub-scene images (X_n'')								Threshold combining		Threshold merging
X_1''	X_2''	X_3''	X_4''	X_5''	X_6''	X_7''	X_8''	Mean	Median	
67	68	67	73	75	70	72	73	70.6	71.0	70.6

specular reflection, corner reflection, and diffuse surface scattering, which is presented in Fig. 12b–g. The category of specular reflection has been presented in this research by the interaction of land-use ALOS PALSAR remotely sensed data signal to the paddy fields areas affected by flood. The object of land use of paddy fields were inundated by floods that tend to have a smooth reflection so that the backscattering signal received by the ALOS
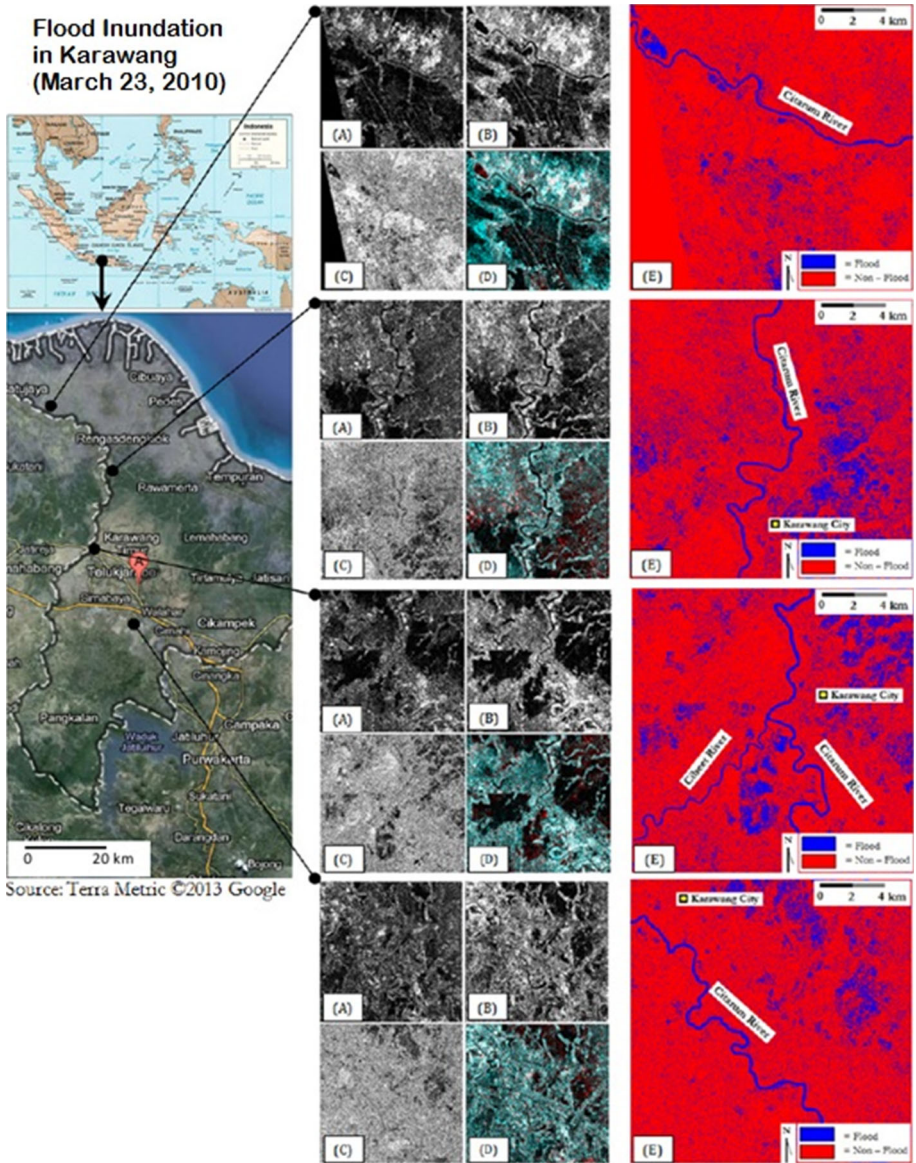
Fig. 11 Map of flood inundation in Karawang. **a** ALOS PALSAR remotely sensed data March 09, 2010 (pre-flood). **b** ALOS PALSAR remotely sensed data March 26, 2010 (post-flood). **c** Result of normalized change index (NCI) based on the calculation of data pre- and post-flood inundation event. **d** False-color composite RGB image pre- and post-flood. R: pre-flood image of ALOS PALSAR remotely sensed data acquired on March 09, 2010. G: post-flood image of ALOS PALSAR remotely sensed data acquired on March 26, 2010. B: post-flood image of ALOS PALSAR remotely sensed data acquired on March 26, 2010. The result of the false-color composite: *Red color* is a flood area; *black to gray to white* is non-flood area. **e** Result of classification of flood and non-flood inundation
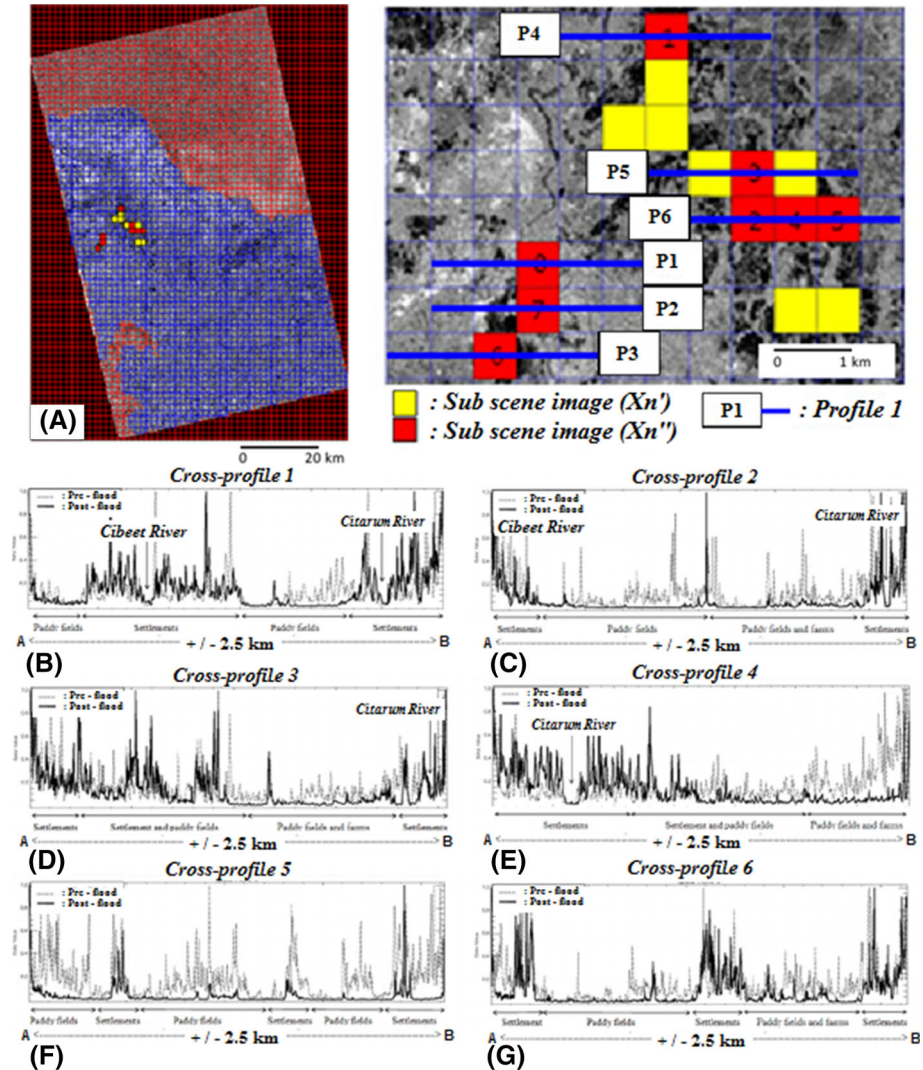
Fig. 12 a Cross-profile location for six transect routes and fields surveys in the research area. Determination of sample six transect routes was carried out at random in accordance with location of sub-scene image (X_n'') for threshold calculation. **b** Difference backscattering value pre- and post-flood in cross-profile 1 (P1). **c** Difference backscattering value pre- and post-flood in cross-profile 2 (P2). **d** Difference backscattering value pre- and post-flood in cross-profile 3 (P3). **e** Difference backscattering value pre- and post-flood in cross-profile 4 (P4). **f** Difference backscattering value pre- and post-flood in cross-profile 5 (P5). **g** Difference backscattering value pre- and post-flood in cross-profile 6 (P6)

PALSAR remotely sensed data sensor to be low and the object seen in the ALOS PALSAR remotely sensed data appeared in dark color compared with the surrounding objects. Backscattering values in pre- and post-flood appear different and more prominent when compared to other land-use objects. It can be seen from Fig. 12b, c, f, g the comparison of backscattering value at pre- and post-flood in the research area. At the time of the pre-
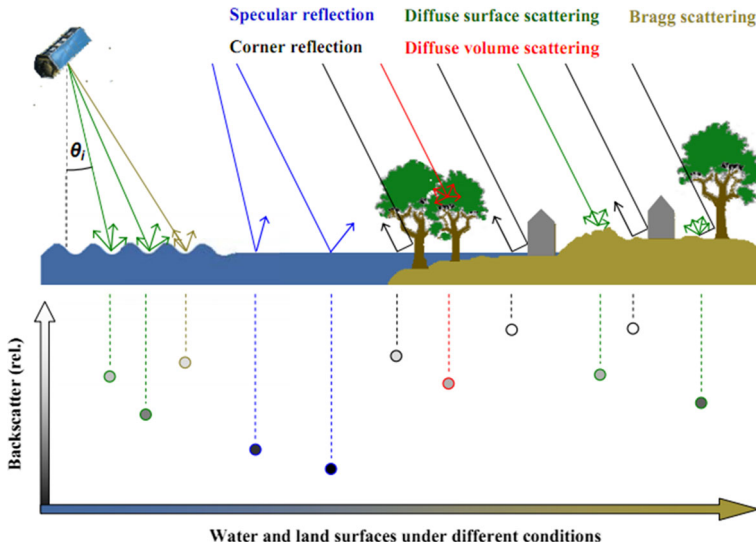
Fig. 13 Backscattering interaction of water and land surfaces between SAR signal (*Source*: Martinis 2010)

flood, objects of land use of paddy fields has values that tend to be high backscattering variations. After inundated by flood, the backscattering value is low as a result of weak backscattering signal received by the sensor ALOS PALSAR remotely sensed data. The category of corner reflection in this research can be shown in the interaction of ALOS PALSAR remotely sensed data signal to a combination of land-use objects of paddy fields and farms, or paddy fields and settlements. It can be seen from Fig. 12c–e, g that the combination of land-use objects of paddy fields and farms, or paddy fields and settlements have a reflection of moderately roughened. This happened because there is the influence of surface roughness that is reflected by the object of supporting the surrounding land use of farms and settlements. So there is a partial signal received by the ALOS PALSAR remotely sensed data sensor, and there are others, which are away from the sensor. In the category of diffuse surface scattering, the interaction can be shown in residential areas affected by floods; in general, it can be seen from Fig. 12b–e, g.

During the investigation, meticulous assessment and observation in each land use and landform unit were carried out. Information from local communities during the profiling and interview activity was very valuable in order to get a description of the environmental problems associated with flood inundation event. Determination of sample six transect routes in this research was carried out at random in accordance with location of sub-scene image (X_n''). Detailed description and information of each cross-profile 1–6 are described as follows:

The cross-profile 1 (Fig. 14) is located in district of Telukjambe, sub-district: Purwadana and district of Karawang, sub-district: Tanjungpura. This profile has distance ±2.5 km from point A to B. The landforms unit is dominated by alluvial plain and fluvial units. The impact of land-use damage is caused by flood inundation event on March 2010, including paddy fields, farms, and settlements. The environmental problems in this profile section consist of flood depth with variations 0.5–1 m in ±0.5 km from point A with land use: paddy fields. Distance area 0.5–1 km from point A has land-use types of settlements with of flood depth variation from 1 up to 2 m, surrounding the Cibeet River. Meanwhile,
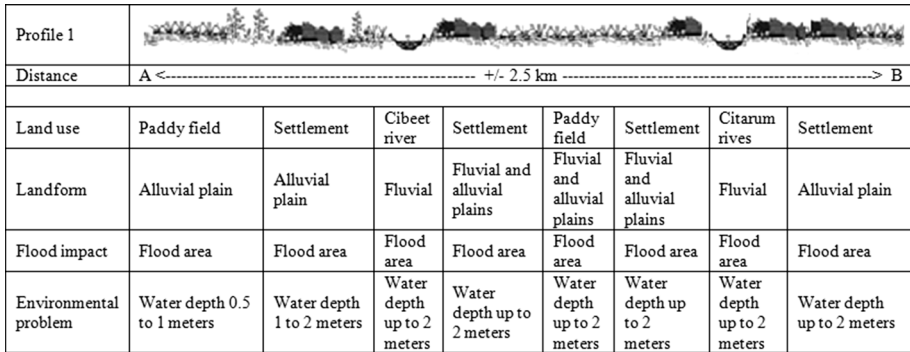
Profile 1								
Distance	A <----------------------------------- +/- 2.5 km -----------------------------------> B							

Land use	Paddy field	Settlement	Cibeet river	Settlement	Paddy field	Settlement	Citarum rives	Settlement
Landform	Alluvial plain	Alluvial plain	Fluvial	Fluvial and alluvial plains	Fluvial and alluvial plains	Fluvial and alluvial plains	Fluvial	Alluvial plain
Flood impact	Flood area	Flood area	Flood area	Flood area	Flood area	Flood area	Flood area	Flood area
Environmental problem	Water depth 0.5 to 1 meters	Water depth 1 to 2 meters	Water depth up to 2 meters	Water depth up to 2 meters	Water depth up to 2 meters	Water depth up to 2 meters	Water depth up to 2 meters	Water depth up to 2 meters

Fig. 14 Cross-profile 1 (P1)

the distance 1–2.5 km from point A has land-use variation, i.e., paddy field and settlement, with variation flood depth up to 2 m, surrounding the Citarum River. The impact of land use is caused by flood inundation event in cross-profile 2 (Fig. 15), including settlement, paddy fields, and farms. This cross-profile is located in the district of Telukjambe, sub-districts: Parungsari, Purwadana and in District Karawang, sub-district: Tanjungpura. In this location, the landforms of alluvial plain and fluvial units are dominant. The environmental problems in this profile section consist of flood depth variation 1–2 m in ±1 km from point A with land use: settlements area surrounding the Cibeet River. In the distance 1–2 km, flood depth variation is up to 2 m with land use: paddy field and farms. Meanwhile, in the distance up to 2 km, it can be shown that variation water depth is up to 2 m with land use: settlement area surrounding the Citarum River.

Cross-profile 3 (Fig. 16) has distance ±2.5 km from point A to B. This cross-profile is located in district of Telukjambe, sub-districts: Mekarmulya, Karanglingar, and Karawang Kulon. Impact of flood includes the following: settlements, paddy fields, and farms, with landform unit that is dominated by fluvial and alluvial plains.

The impact of flood inundation on cross-profile 4 (Fig. 17) is appeared at a distance ±1 km from point A with land use: Settlement area surrounding the Citarum River has variation of water depth up to 2 m. Impact of flood is dominated by paddy fields, farms, and settlements with water depth 0.5–2 m. This profile is located in district of Rengasdengklok, sub-districts: Kalangsari, Kalangsurya, and Sindangmukti.

Profile 2								
Distance	A <----------------------------------- +/- 2.5 km -----------------------------------> B							

Land use	Settlement	Cibeet river	Settlement	Paddy field	Paddy field and farms	Settlement	Citarum rives	Settlement
Landform	Fluvial and alluvial plains	Fluvial	Fluvial and alluvial plains	Alluvial plains	Alluvial plains	Fluvial and alluvial plains	Fluvial	Fluvial and alluvial plains
Flood impact	Flood area	Flood area	Flood area	Flood area	Flood area	Flood area	Flood area	Flood area
Environmental problem	Water depth 0.5 to 1 meters	Water depth 1 to 2 meters	Water depth up to 2 meters	Water depth up to 2 meters	Water depth up to 2 meters	Water depth up to 2 meters	Water depth up to 2 meters	Water depth up to 2 meters

Fig. 15 Cross-profile 2 (P2)

Profile 3						
Distance	A <--- +/- 2.5 km ---> B					

Land use	Settlement	Settlement and paddy field	Paddy field and farms	Settlement	Citarum rives	Settlement
Landform	Alluvial plains	Alluvial plains	Alluvial plains	Fluvial and alluvial plains	Fluvial	Fluvial and alluvial plains
Flood impact	Flood area	Flood area	Flood area	Flood area	Flood area	Flood area
Environmental problem	Water depth 0.5 to 1 meters	Water depth 1 to 2 meter	Water depth up to 2 meters	Water depth up to 2 meters	Water depth up to 2 meters	Water depth up to 2 meters

Fig. 16 Cross-profile 3 (P3)

Profile 4				
Distance	A <--- +/- 2.5 km ---> B			

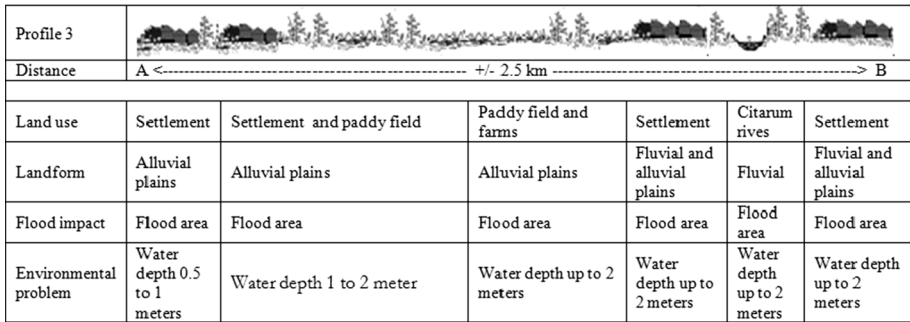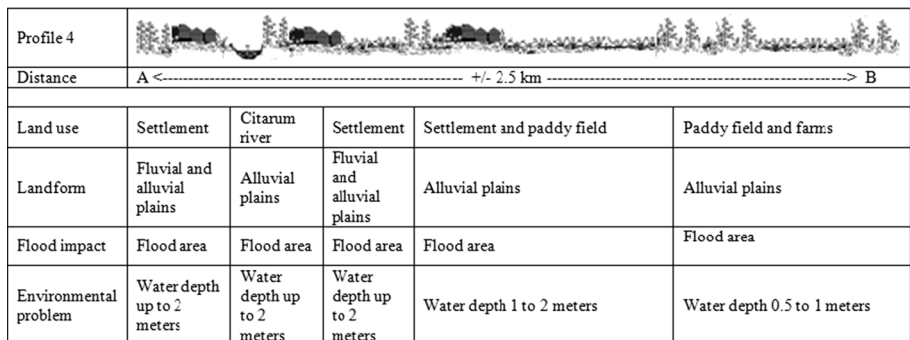|				
Land use	Settlement	Citarum river	Settlement	Settlement and paddy field	Paddy field and farms
Landform	Fluvial and alluvial plains	Alluvial plains	Fluvial and alluvial plains	Alluvial plains	Alluvial plains
Flood impact	Flood area	Flood area	Flood area	Flood area	Flood area
Environmental problem	Water depth up to 2 meters	Water depth up to 2 meters	Water depth up to 2 meters	Water depth 1 to 2 meters	Water depth 0.5 to 1 meters

Fig. 17 Cross-profile 4 (P4)

The cross-profile 5 (Fig. 18) has landform unit dominated by alluvial plain. This profile is located in the district of Karawang, sub-districts: Rawamerta, Pasirkaliki, and Kutawargi. Variation of land use is dominated by paddy fields and settlements. Impact of flood and water depth 0.5–1 m is distributed from point A to B with distance ±2.5 km.

The land use in cross-profile 6 (Fig. 19) is dominated by settlements, paddy fields, and farms. This profile is located in the district of Karawang, sub-districts: Karawangpawitan, Palumbonsari, and Plawad, with landforms dominated by alluvial plains. Variation of water depth 0.5–1 m is distributed from point A to B, with environmental problems in land-use settlement, paddy fields, and farms.

The highest impact of flood inundation event on March 2010 is dominated by paddy fields and settlements. This flood is estimated (Table 6) to have an impact of 7,158 ha for settlements; 20,039 ha for paddy fields; 668 ha for plantations; 1,641 ha for farms; 198 ha for agricultural cultivations; 1,161 ha for shrubberies; 1,022 ha for industrials; and 1,019 ha for road areas. Table 6 shows the damage impact on land-use area of the flood inundation event on March 2010 in the research area.

The damage impacts of land use of settlements were greatest in the districts of Karawang, Klari, and Telukjambe (Fig. 20), with value: 1,751; 1,457; and 1,269 ha, respectively. Based on the Statistic of Karawang (2011), these districts have number of population: 273,472 people; 155,336 people; and 175,419 people, respectively, in year 2010 (Table 1). While, damage impacts of land use of paddy fields were greatest in districts of Telukjambe, Klari, Karawang,
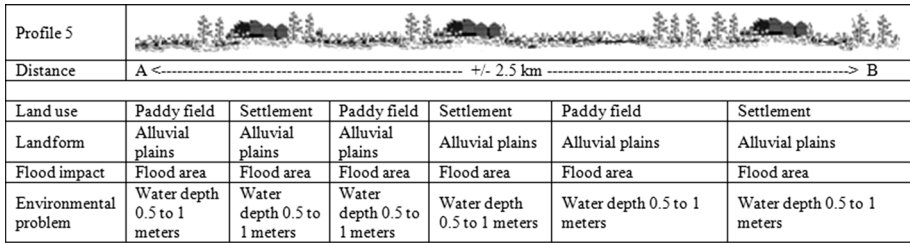
Profile 5						
Distance	A <--- +/- 2.5 km ---> B					

Land use	Paddy field	Settlement	Paddy field	Settlement	Paddy field	Settlement
Landform	Alluvial plains	Alluvial plains	Alluvial plains	Alluvial plains	Alluvial plains	Alluvial plains
Flood impact	Flood area	Flood area	Flood area	Flood area	Flood area	Flood area
Environmental problem	Water depth 0.5 to 1 meters	Water depth 0.5 to 1 meters	Water depth 0.5 to 1 meters	Water depth 0.5 to 1 meters	Water depth 0.5 to 1 meters	Water depth 0.5 to 1 meters

Fig. 18 Cross-profile 5 (P5)

Profile 6					
Distance	A <--- +/- 2.5 km ---> B				

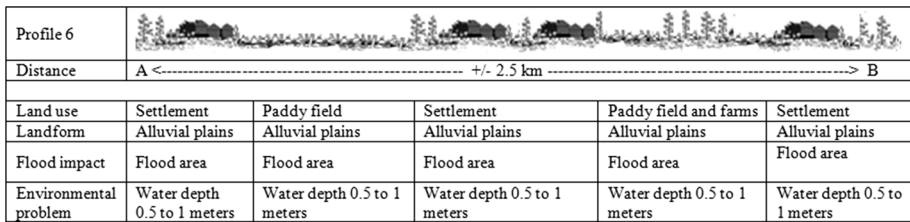| Land use	Settlement	Paddy field	Settlement	Paddy field and farms	Settlement
Landform	Alluvial plains	Alluvial plains	Alluvial plains	Alluvial plains	Alluvial plains
Flood impact	Flood area	Flood area	Flood area	Flood area	Flood area
Environmental problem	Water depth 0.5 to 1 meters	Water depth 0.5 to 1 meters	Water depth 0.5 to 1 meters	Water depth 0.5 to 1 meters	Water depth 0.5 to 1 meters

Fig. 19 Cross-profile 6 (P6)

Rengasdengklok, and Rawamerta, with value: 4,144; 4,026; 3,810; 2,488; and 2,218 ha, respectively. In this research, the total number of building damages is estimated to be around 16,350 units (Table 7). The highest damage impact is estimated 4,611 units in the district of Karawang; 4,033 units in Klari; 3,572 units in Telukjambe; 1,417 units in Rengasdengklok; 644 units in Batujaya; 600 units in Rawamerta; 478 units in Tritamulya; 406 units in Cikampek; 372 units in Talagasari; and 217 units in Pakisjaya.

The calculation of the impact of flood inundation event on land use in the research area is estimated, but the results of the calculations can be used as an initial step and rapid method for estimating the magnitude of damage caused by disasters. For the next future research, the assessment of the risk and damage in terms of economic losses can be calculated based on the current market value in that area.

6 Conclusions

Rapid mapping is needed for emergency response in disaster mitigation efforts, especially flood. This was done as a contribution in determining policy and the next steps after the flood, such as an evacuation route planning, determining the location of distribution logistics, and others. In the rainy season conditions, the acquisition and availability of optical remote sensing data that are clear of cloud cover tend to be difficult to obtain. This can be a major problem in flood monitoring using remote sensing data. The objects that would otherwise be detected and recorded by a remote sensing data are visible as it is covered by clouds. The uses of ALOS PALSAR remotely sensed data can be used as an alternative solution to overcome it. In this research, multi-temporal ALOS PALSAR remotely sensed data with a medium-size resolution have been used to detect areas affected by floods in the research area. Application of change detection in multi-temporal ALOS PALSAR remotely sensed data has been successfully carried out to make the flood inundation map, based on

Table 6 Damage impact on land use and district area in Karawang of the flood inundation event on March 2010

No.	Districts	Types of land use—area in hectares (ha)							
		Settlements	Paddy fields	Plantations	Farms	Agricultural cultivations	Shrubberies	Industrials	Roads
1	Batujaya	544	745	3	74	0.2	13	–	66
2	Cikampek	262	730	83	183	11	190	236	48
3	Karawang	1,751	3,810	91	57	19	67	–	213
4	Klari	1,457	4,026	189	385	67	496	–	218
5	Pakisjaya	83	339	25	0.7	83	17	–	23
6	Rawamerta	431	2,218	19	–	0.4	–	–	55
7	Rengasdengklok	937	2,488	50	253	5	28	–	107
8	Talagasari	156	614	5	–	0.1	7	–	31
9	Telukjambe	1,269	4,144	198	637	12	335	785	219
10	Tritamulya	268	925	16	52	0.4	9	–	41
	Total	7,158	20,039	668	1,641	198	1,161	1,022	1,019
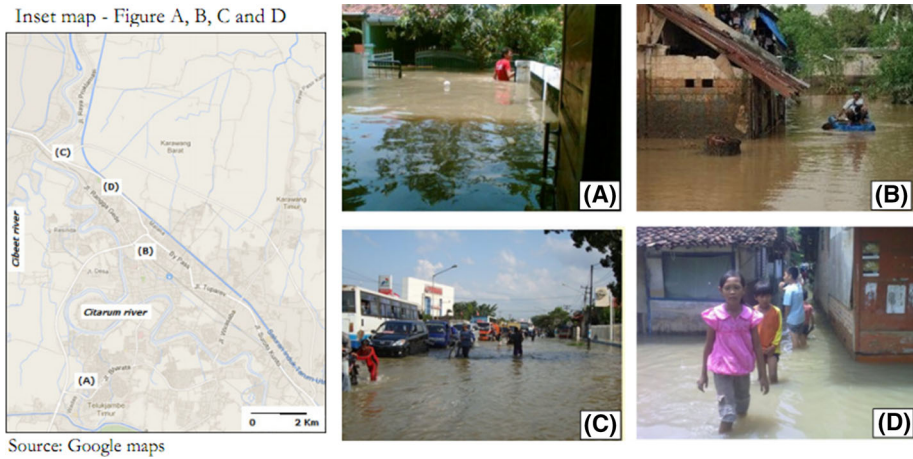
Fig. 20 Damage impact of the flood inundation event on March 2010. **a** Flood inundation with water depth 1–2 m in a residential Karawang Barat Indah, Telukjambe (*source photo*: DPB. March 25, 2010). **b** Inundation with water depth up to 2 m in the district of Karawang (*source photo*: TE Yanuarti. March 25, 2010). **c** Floods inundated roads in Tanjungpura, district of Karawang. **d** Floods in settlements area, located in Paraci, Tanjungpura, Karawang (*source photo* **c**, **d**: Tatang. March 25, 2010)

Table 7 Damage impact on building area of the flood inundation event on March 2010 in the research area

No.	Districts	No. of damaged building area (units)
1	Batujaya	644
2	Cikampek	406
3	Karawang	4,611
4	Klari	4,033
5	Pakisjaya	217
6	Rawamerta	600
7	Rengasdengklok	1,417
8	Talagasari	372
9	Telukjambe	3,572
10	Tritamulya	478
Total		16,350

the identification of changes in the backscattering value at the time of pre-flood and post-flood. The changes of the backscattering value can be rapidly and effectively done using a calculation of normalized change index. Split-based approach has been used in this research to obtain the average variation of the local threshold value, which can then be used to calculate the global threshold value in one scene ALOS PALSAR remotely sensed data. The use of the threshold value is able to classify the areas affected by floods, in the class of "flood" and "non-flood," which is based on the calculation of the minimum error principle of Kittler and Illingworth approach. Although the ALOS PALSAR remotely sensed data have been successfully used in this research for mapping of inundated areas globally, there are also some limitations: Some of the areas with the local flood conditions and the

distribution of flood in relatively small area are still difficult to detect. This can occur due to the limited spatial resolution that is owned by the data used in this research. These limitations, the use of SAR remote sensing data with better resolution and detail is recommended for the next future research. Identification and assessment of environmental damage focus on the calculation of the land-use area affected by flood inundation event. This is done to get a general overview of the impact of flood inundation event in the research area (flood hazard assessment). The use of overlay method using a GIS environment tool against flood inundation maps and land-use information, and transect surveys or cross-profile on the ground observation in selected locations has been used to effectively describe the general condition of the impact of flood inundation event in the research area. The results of this research can be used and recommended for future research, in taking into account more detailed information related to the impact of flood inundation event in the research area (application to flood damage assessment). It can also be performed for the development of other research, such as the assessment of the risk and damage in terms of economic losses, which can be calculated based on current market value in the research area. In addition, the use of the method can also be applied at different locations, for quick response and rapid mapping in the events of other disasters, such as flash floods, landslide, tsunami, volcano eruptions, and forest fire.

References

Bayarsaikhan U, Boldgiv B, Kim KR, Park KA, Lee D (2009) Change detection and classification of land cover at Hustai National Park in Mongolia. Int J Appl Earth Obs Geoinf 11:273–280

Bazi Y, Bruzzone L, Melgani F (2005) An unsupervised approach based on generalized gaussian model to automatic change detection in multitemporal SAR image. IEEE Trans Geosci Remote Sens 43(4):874–886. doi:10.1109/TGRS.2004.842441

Billa L, Mansor S, Mahmud AR, Ghazali AH (2006) Modelling rainfall intensity from NOAA AVHRR data for operational flood forecasting in Malaysia. Int J Remote Sens 27(23):5225–5234

Blasco F, Bellan MF, Chaudhury MU (1992) Estimating the extent of floods in Bangladesh using SPOT data. Remote Sens Environ 39:167–178

Bovolo F, Bruzzone L (2007) A split-based approach to unsupervised change detection in large-size multitemporal images: application to tsunami-damage assessment. IEEE Trans Geosci Remote Sens 45(6):1658–1670. doi:10.1109/TRGS.2007.895835

Brakenridge R, Anderson E (2006) MODIS-based flood detection, mapping and measurement: the potential for operational hydrological applications. In: Marsalek J et al (Eds) Transboundary floods: reducing risks through flood management. Springer, Netherlands, pp 1–12

Brivio PA, Gregoire JM, Zilioli E (1984) The detection of hydrological indicators in the study of Niger river regime by means of Landsat imageries. ITC J 3:191–199

Brivio PA, Colombo R, Maggi M, Tomasoni R (2002) Integration of remote sensing data and GIS for accurate mapping of flood areas. Int J Remote Sens 23(3):429–441. doi:10.1080/01431160010014729

Development Planning Board (DPB) (2011) Profile of Karawang RPJMD 2011–2015. Government of Karawang, Indonesia (in Indonesian)

Dong Y, Li Q, Dou A, Wang X (2010) Extracting damages caused by the 2008 Ms 8.0 Wenchuan earthquake from SAR remote sensing data. J Asian Earth Sci 40:907–914. doi:10.1016/j.jseaes.2010.07.009

Huang S, Cai X, Chen X, Liu D (2011) Change detection method based on fractal model and wavelet transform for multitemporal SAR images. Int J Appl Earth Obs Geoinf 13:863–872. doi:10.1016/j.jag.2011.05.018

Kittler J, Illingworth J (1986) Minimum error thresholding. Pettern Recognit 19(1):41–47

Kuligowski RJ (2011) Satellite rainfall information for flood preparedness and response. In: Use of satellite and in situ data to improve sustainability NATO science for peace and security series C: environmental security, pp 31–39

Lougeay R, Baumann P, Nellis MB (1994) Two digital approaches for calculating the area of regions affected by the great American flood of 1993. Geocarto Int 9:53–59

Marfai MA (2011) Impact of coastal inundation to ecology and agricultural land use, case in Central Java Indonesia. Int J Quaest Geogr 30(3):19–32

Marfai MA, King L (2008) Potential vulnerability implications of coastal inundation due to sea level rise for coastal zone of Semarang City, Indonesia. Environ Geol 54(6):1235–1245

Martinis S (2010) Automatic near real-time flood detection in high resolution X-band synthetic aperture radar satellite data using context-based classification on irregular graphs. Dissertation, Fakultät für Geowissenschaften, Ludwig-Maximilians-Universität München

Martinis S, Twele A, Voigt S (2009) Toward operational near real-time flood detection using a split-based automatic threshold procedure on high resolution TerraSAR-X Data. Nat Hazard Earth Syst Sci 9:303–314

Mason DC, Speck R, Devereux B, Schumann GJP, Neal JC, Bates PD (2010) Flood detection in urban areas using TerraSAR-X. Geosci Remote Sens IEEE Trans 48:882–894

Moser G, Serpico SB (2006) Generalized minimum-error thresholding for unsupervised change detection from SAR amplitude imagery. Geosci Remote Sens IEEE Trans 44(10):2972–2982

Pantaleoni E, Engel BA, Johannsen CJ (2007) Identifying agricultural flood damage using Landsat imagery. Precision Agric 8(1–2):27–36

Quan W, Masataka W, Seiji H, Shogo M (2003) Using NOAA AVHRR data to assess flood damage in China. Environ Monit Assess 82(2):119–148

Sanjay KJ, Arun KS, Ajanta G, Tanvear A (2006) Flood inundation mapping using NOAA AVHRR data. Water Resour Manage 20(6):949–959

Shifeng H, Jinggang L, Mei X (2012) Water surface variations monitoring and flood hazard analysis in Dongting Lake area using long-term Terra/MODIS data time series. Nat Hazard 62(1):93–100

Singh A (1989) Digital change detection techniques using remotely-sensed data. Int J Remote Sens 10(6):989–100

Smith K, Ward R (1998) Floods: physical processes and human impact. Wiley, Chichester

Statistic of Karawang (2011) Government of Karawang. http://www.karawangkab.go.id. Cited 01 Oct 2012

Sutikno S (2007) Earthquake disaster of Yogyakarta and Central Java, and disaster reduction, Indonesia. Forum Geogr 21(1):1–16

The Indonesian National Agency for Disaster Management (BNPB) (2012) Disaster information data in Indonesia. http://www.bnpb.go.id. Cited 05 July 2012

The Regional Agency for Disaster Management (BPBD)—Province of West Java (2011) Recapitulation of disaster in West Java, Indonesia. http://www.bpbd.jabarprov.go.id. Cited 07 Mar 2012

Townsend PA (2001) Mapping seasonal flooding in forested wetlands using multi-temporal Radarsat SAR. Photogram Eng Remote Sens 67:857–864

Tzeng CJ, Lin YH, Yang YK, Jeng MC (2009) Optimization of turning operations with multiple performance characteristics using the Taguchi method and Grey relational analysis. J Mater Proces Technol 209(6):2753–2759

Ward PJ, Marfai MA, Yulianto F, Hizbaron DR, Aerts JCJH (2011) Coastal inundation and damage exposure estimation: a case study for Jakarta. Nat Hazards 56:899–916

Wulder MA, White JC, Goward SN, Masek JG, Irons JR, Herold M, Cohen WB, Loveland TR, Curtis E. Woodcock CE (2008) Landsat continuity: issues and opportunities for land cover monitoring. Remote Sens Environ 112(3):955–969

Yueming Q, Haiqiao T, Xing L (2007) Geomorphologic study of anhui section of Changjiang River using Landsat TM image. Chin Geogr Sci 17(3):250–256

Yulianto F, Sofan P, Khomarudin MR, Haidar M (2013) Extracting the damaging effect of the 2010 eruption of Merapi volcano in Central Java, Indonesia. Nat Hazards 66:229–247. doi:10.1007/s11069-012-0438-4